LBNL-46526

ERNEST ORLANDO LAWRENCE
BERKELEY NATIONAL LABORATORY

A High-Rate Manganese Oxide for Rechargeable Lithium Battery Applications

Marca M. Doeff, Abraham Anapolsky, Ludvig Edman, Thomas J. Richardson, and L.C. DeJonghe

Materials Sciences Division

July 2000

Submitted to *Journal of the Electrochemical Society*

DISCLAIMER

A High-Rate Manganese Oxide for Rechargeable Lithium Battery Applications

Marca M. Doeff[a], Abraham Anapolsky[a], Ludvig Edman[c], Thomas J. Richardson[b], and L.C. De Jonghe[a]

[a] Materials Sciences Division

[b] Environmental Energy Technologies Division

Lawrence Berkeley National Laboratory

University of California

Berkeley, CA 94720

and

[c] Department of Experimental Physics

Umeå University, S-90187 Umeå, Sweden

Acknowledgments

This work was supported by the Assistant Secretary for Energy Efficiency and Renewable Energy, Office of Transportation Technologies, Office of Advanced Automotive Technologies of the U.S. Department of Energy under Contract No. DE-AC03-76SF00098. We would like to thank Dr. Xiao-Feng Zhang of the Materials Sciences Division for providing TEM images and for helpful discussion.

Abstract

Li_xMnO_2 made by ion-exchange of glycine-nitrate combustion synthesis-produced orthorhombic $Na_{0.44}MnO_2$ (GNP-Li_xMnO_2) has been cycled in lithium/liquid electrolyte cell configurations at room temperature and lithium/polymer cell configurations at 85° C over one hundred times without showing capacity fading or phase conversion to spinel. At 2.5 mA/cm^2 in liquid cells (5C rate) or 1 mA/cm^2 (1.5C rate) in polymer cells, 80-95% of the expected capacity is delivered. The remarkable stability is attributable to the unusual double tunnel structure, which cannot easily undergo rearrangement to spinel. The enhanced rate capability of GNP-Li_xMnO_2 compared to conventionally prepared materials is attributable to the shorter particle length, which allows faster diffusion of lithium ions along the tunnels.

Introduction

The low raw materials price of manganese oxide ($1.04/lb[1]) compared to cobalt oxide ($18-19/lb) provides a compelling reason to pursue the former as cathodes for electric or hybrid electric vehicle (EV or HEV) batteries, where the cost constraints are severe. The polymorphous nature and phase instability of the manganese oxide system have, however, complicated the quest, especially considering the extreme demands of these applications. According to the long-term goals of the U.S. Advanced Battery Consortium (USABC), EV batteries must be able to undergo at least 1000 cycles to 80% depth-of-discharge, last ten years, tolerate both over-charge and -discharge (preferably without electronic controls), and operate at temperatures ranging from -30 to 65° C. While high energy density is needed for EVs, high power density is more critical for HEVs; power-to-energy ratios of about 2 are needed for the former but 5-20 for the latter, along with the ability to withstand tens of thousands of shallow cycles.[2]

Most work on manganese oxides for rechargeable lithium batteries has focused on development of $LiMn_2O_4$ and related spinels. $LiMn_2O_4$ cycles with only a slight capacity fade at room temperature.[3] Dissolution of manganese ions and concomitant formation of defect spinel near the end of charge are responsible for the loss of 4V capacity.[4] At 55° C or above, dissolution is accelerated, resulting in poor cycling at elevated temperatures.[5] Other phenomena that can contribute to fading include the large anisotropic distortion associated with a cooperative Jahn-Teller induced tetragonal phase change that occurs for $x>1$ in $Li_xMn_2O_4$. This may happen either when cells are discharged normally to 3V, or under high rate, non-equilibrium conditions on the 4V plateau.[6] The sensitivity of lithium

manganese oxide spinels to damage during high rate discharge, over-discharge, or at elevated temperatures, contra-indicate their use in traction applications where such abuses are likely to occur.

Layered manganese oxides are also under investigation for battery applications.[7,8] Many of these are prepared as ternary compounds containing either Na or K ions, and are used as is or exchanged prior to incorporation in a lithium cell. Most layered compounds have structural features in common with spinels and convert readily upon cycling. Work is underway in several groups to improve the meta-stability by admetal doping or by pillaring the layers[9]. Alternatively, layered compounds that do not have cubic close-packed arrays of oxygen may prove to be more resistant to spinel conversion, but can undergo other irreversible phase transitions during the first few cycles.[10]

Layered oxides and most tunnel-type oxides are incapable of accommodating the tetragonal Jahn-Teller distortion that occurs on reduction of Mn(IV) to Mn(III). These structures consist of rigid blocks of close-packed oxide ions with manganese in octahedral sites. The local symmetry of the manganese ions in these blocks is trigonal. Cooperative rearrangement of these structural units to accommodate tetragonally elongated octahedral coordination creates sufficient strain to activate the conversion to the stable, tetragonal Mn(III) spinel. Less rigid manganese oxide structures, and those not based on a cubic close-packed array of oxygen ions, are much more likely to remain phase-stable upon cycling in a lithium cell configuration.

One such structure is that based on the double-tunnel compound $Na_{0.44}MnO_2$.[11,12] (Figure 1). $Na_{0.44}MnO_2$ contains both MnO_6 octahedra and MnO_5 square pyramids, which act as hinges to accommodate strain during lithium insertion or de-insertion, and the

accompanying changes in Mn-O coordination. Ion-exchanged materials cycle with no capacity fading in a lithium cell configuration[13] and are unusually resistant to degradation when over-charged or over-discharged.[14] Furthermore, conversion to the spinel structure does not occur below about 400° C. These features make Li_xMnO_2 with the $Na_{0.44}MnO_2$ structure especially attractive for use in demanding HEV and EV battery applications.

Experimental

$Na_{0.44}MnO_2$ was synthesized by a glycine-nitrate process (GNP) according to the method of Chick et al.[15] An Na/Mn ratio of 0.49 was initially used to compensate for sodium losses during combustion, and to minimize production of Mn_2O_3 impurities. The resultant fine powder was calcined at 800° C for four hours, and then reground and re-fired at the same temperature for four hours two more times to ensure sample homogeneity. X-ray analysis using a Siemens D5000 diffractometer indicated that the product was phase-pure and did not contain Mn_2O_3. $Na_{0.44}MnO_2$ was also produced by heating intimately mixed Na_2CO_3 and Mn_2O_3 powders together, with an Na/Mn ratio of 0.44, at 800° C for eight hours. The xrd pattern indicated that the resultant powder contained about 20% Mn_2O_3 by weight. An aqueous solution of NaOH in an amount sufficient to react with the Mn_2O_3 impurity completely was then added and the powder re-fired for another eight hours. This was sufficient to produce a phase-pure material.

Surface area analysis by BET was carried out on both samples by Micromeritics, Norcross, GA. Scanning electron microscopy (Microspec ISI-DS 130C dual stage SEM) was used to observe the particle morphology of both samples.

$Na_{0.44}MnO_2$ powders were ion-exchanged by heating them in a molten salt mixture of 68 mol% $LiNO_3$/32 mol% KNO_3 at 230-250° C. A 2-5-fold excess of the Li salt was used, and the supernatant liquid was poured out and replaced twice during the exchange, which typically took 48 hours. Exchanges were determined to be complete by XRD analysis and by atomic absorption analysis (S. Mountford, Earth Sciences Division, Lawrence Berkeley National Laboratory, Berkeley, CA). Exchanged samples were phase-pure and isomorphous to the parent compounds. Li_xMnO_2 derived from glycine-nitrate process $Na_{0.44}MnO_2$ is designated GNP-Li_xMnO_2 and that derived from the conventional solid state synthesis is designated SS-Li_xMnO_2.

Cells were assembled by stacking porous electrodes containing the active material, C black and EPDM binder on stainless steel or graphite foil discs, Celgard 3401, lithium metal (Cyprus-Foote Mineral Co., Kings Mountain, NC), metal backing plates, and wave washers in 2032 coin cells and pressing together, after wetting with electrolyte solution (1M $LiPF_6$ in 1:2 EC-DMC, EM Industries, Darmstadt, Germany). Composite polymer electrodes and polymer cells were fabricated as described previously.[11] Polyethylene oxide (PEO, Aldrich, M_v = $5 \cdot 10^6$ g/mol) complexed with lithium (bis)trifluoro-methanesulfonate imide (LiTFSI, 3M Company) in an 8:1 molar ratio (designated $P(EO)_8$LITFSI) was used in both cathode and separators. Typical loadings for both types of electrodes were approximately 5 mg/cm^2 of active material.

Polymer cells were equilibrated at 85±0.5° C in a convection oven equipped with a Eurotherm controller for at least one hour prior to testing. A MacPile II (Bio-Logic, SA, Claix, France) was used for both galvanostatic and potentiostatic experiments. For electrochemical potential spectroscopy experiments (ECPS), the potential was stepped 10

mV every 4 hours, or until the current had decreased to 1/1000 of its initial value, between 2.6 and 3.5V for polymer cells and between 2.5 and 3.8 V for liquid electrolyte cells.

Results and Discussion

Figure 2 shows a differential capacity plot obtained from an ECPS experiment on a Li/1M $LiPF_6$ EC-DMC/SS-Li_xMnO_2 cell at room temperature. For this sample, only two major sets of peaks are evident. The number, positions, intensities and widths of the peaks vary considerably with sample preparation, extent-of-exchange, and operating temperature, but always show good reversibility, provided that the potential is kept above about 2.5V. For incompletely exchanged samples, additional peaks belonging to a secondary sodium-containing phase are often seen. The absence of minor peaks in this sample provide additional confirmation of complete exchange.

Relative Li ion diffusion coefficients as a function of cell potential (state-of-charge) can be calculated from i vs. t data for each 10 mV step in the ECPS experiment, by applying the Cottrell equation (Figure 3). Because the positive electrode is porous and the contact area between the active material and electrolyte solution is not known, it was not possible to calculate true diffusion coefficients; thus no numerical values are given. Still, the trends as a function of cell state-of-charge seen in Figure 3 are instructive in understanding the behavior of this manganese oxide. Diffusion is fastest in the middle of discharge, and is slower by several orders of magnitude when the cell is nearly fully charged. It also slows markedly at the end of discharge; presumably when the tunnels are nearly full. This results in rate limitations and/or lower utilization than expected when

cells containing cathode materials with long diffusion path-lengths (e.g., large average particle size) are cycled between set voltage limits.

Evidence of rate limitations are seen when Li/1M $LiPF_6$ EC-DMC/SS-Li_xMnO_2 cells are discharged at 0.5 mA/cm^2 and compared to the pseudo-open circuit profile obtained by integrating the differential capacity data from the ECPS experiment (Figure 4). The pseudo-OCP profile is gradually sloping with two prominent plateaus (corresponding to the sharp peaks in the differential capacity plot) with a capacity of slightly over 100 mAh/g between 3.8 and 2.5V. The galvanostatic discharge, in contrast, has a lower average voltage, the plateaus are less apparent, and utilization is only about 80% of the expected amount. In contrast, Li/1M $LiPF_6$ EC-DMC/GNP-Li_xMnO_2 cells deliver the full capacity at the same current density with well-defined discharge profiles and little voltage penalty.

Differences in the particle morphologies and sizes of SS-Li_xMnO_2 and GNP-Li_xMnO_2 account for the improved performance of the latter (Figure 5a and b). SS-Li_xMnO_2 particles have a needle-like morphology, with a length of about 4-5 μm. A TEM study[16] on this material indicates that the tunnels are aligned parallel to the long axis of the needles (Figure 6). Since diffusion is expected to be highly anisotropic, reduction of particle size in this dimension has a much greater effect on performance than over-all increased surface area or a reduction in the other dimensions.[17] The needles of the GNP-Li_xMnO_2 sample are significantly shorter (1 μm or less), although the surface area is probably somewhat lower than that of the SS-Li_xMnO_2, assuming no changes in the surface area occurred during ion-exchange (1.17 M^2/g was obtained for GNP-$Na_{0.44}MnO_2$ and 2.03 M^2/g for SS-$Na_{0.44}MnO_2$). The lower surface area of the GNP product is, most

likely, attributable to the repeated post-combustion grinding and annealing cycles necessary for ensuring the phase purity, which caused some particles to fuse together but did not increase their length. A high surface area can increase the rate of side-reactions such as electrolyte oxidation, and presents a safety hazard under some circumstances; thus the combination of enhanced diffusion without increased surface area is a highly desirable feature of the GNP-Li_xMnO_2 material.

Several consecutive discharges of liquid electrolyte cells containing GNP-Li_xMnO_2 at various rates are shown in Figure 7. Full utilization is seen at 80 $\mu A/cm^2$ and 0.5 mA/cm^2, and only a small decrease is seen at 0.8 mA/cm^2 (this cell also appeared to condition somewhat, resulting in slight improvement as it was cycled). Figure 8 shows discharges at various current densities later in the cycling, when wider voltage limits were used. This resulted in a somewhat higher discharge capacity of about 120 mAh/g for low to moderate rates, but the voltage characteristics were more dependent upon current density than for the earlier discharges. However, it was still possible to discharge this cell at 2.5 mA/cm^2 (5C rate) and obtain nearly the full capacity.

Figure 9a shows the capacity of the same cell as a function of discharge number for cycles 28-107 at a current density of 0.14 mA/cm^2. (Earlier cycles are omitted because of the variation in conditions used). Figure 9b shows later cycling data, including the discharges carried out at 2.5 mA/cm^2. Although utilization decreased somewhat during the high rate cycling, it was recovered during subsequent discharges at lower current densities, indicating that the cathode material was not damaged by this regime. Slightly less capacity is obtained for this cell when it is cycled at 0.5 mA/cm^2 than at 0.14 mA/cm^2, but the excellent capacity retention is still evident, with no signs of fading.

These experiments quite clearly illustrate the remarkable reversibility and stability of Li_xMnO_2 made from $Na_{0.44}MnO_2$.

Improved rate capability and cycling behavior can also be obtained on SS-Li_xMnO_2 electrode materials that have been attritor-milled for three hours prior to use. Figure 10 shows capacity as a function of discharge number at room temperature for a Li/liquid electrolyte cell containing attritor-milled SS-Li_xMnO_2. A very slight fade is seen and there appears to be somewhat more dependence of utilization upon the current density than for GNP-Li_xMnO_2. This can be partially attributed to the different voltage limits used when cycling this cell; in particular, repeated discharging below about 2.5V can result in some capacity loss[12] (this, however, depends upon current density, temperature, and sample preparation technique). While attritor-milling appeared to reduce the average particle size of the SS-Li_xMnO_2, it did not necessarily decrease the length of the needles as the GNP synthetic procedure did (rather, it tended to splinter the particles). Thus, the particle morphology is not as well-optimized, and this is reflected in the slightly poorer performance.

Figure 11 shows a differential capacity plot from a stepped potential experiment performed on a Li/$P(EO)_8$LiTFSI/GNP-Li_xMnO_2 cell between 3.5 and 2.6V at 85° C. The elevated temperature is necessary to render $P(EO)_8$LiTFSI sufficiently conductive, and more conservative voltage limits for the ECPS experiment were chosen because of the susceptibility of the polymer electrolyte to oxidation. The discharge characteristics of the polymer cells are similar to that of those containing liquid electrolytes, although there is slightly higher capacity between 3.6 and 2.5V (Figure 12), at low to moderate rates. Approximately 100 mAh/g is obtained at 0.1-0.2 mA/cm^2, which decreases about 20%

when the current is increased to 1 mA/cm^2. The liquid electrolyte results indicate that the cathode active material is not the limiting factor in the performance of the polymer electrolyte cells. Although the conductivity of $P(EO)_8LiTFSI$ is fairly high at 85° C (6.3 x 10^{-4} S/cm), the non-unity transference number (0.45) and the very slow dissipation of salt concentration gradients in polymer electrolytes limit the current density at which cells can be discharged.[18,19]

Cycling results for a Li/$P(EO)_8LiTFSI$/GNP-Li_xMnO_2 cell at 85° C, discharged at 0.5 mA/cm^2 (1.5C rate), are presented in Figure 13. Remarkably, almost no capacity loss is seen over 140 discharges, indicating that Li_xMnO_2 made from $Na_{0.44}MnO_2$ can be cycled at elevated temperatures, even in the presence of a somewhat acidic electrolyte. This is in sharp contrast to $LiMn_2O_4$ which loses capacity rapidly above 55° C.

It is particularly striking that cycling more capacity is not associated with a higher fade rate in cells containing Li_xMnO_2 electrodes. In fact, GNP-Li_xMnO_2 cycles better than SS-Li_xMnO_2, in both liquid and polymer cell configurations, even though higher capacity is utilized. The performance of SS-Li_xMnO_2 electrodes also appears to be more sensitive to the lower voltage cut-off and to the current density used. For example, SS-Li_xMnO_2 exhibits an average loss of 0.2% of its capacity per cycle in a polymer cell, when discharged at 0.2 mA/cm^2 between 3.6 and 2.5 V, compared to 0.02% for the GNP-Li_xMnO_2 cell in Figure 13, discharged at 0.5 mA/cm^2. The poorer cycling behavior can be attributed to inadvertent over-reduction of Li_xMnO_2 on the surface of particles, due to the sluggish lithium ion diffusion near the end of discharge. During over-reduction, a very slow irreversible conversion to another, unknown, electro-active phase occurs.[14] This new phase inserts lithium reversibly, but has poorer electrochemical properties than the parent

compound; its formation thus causes slow capacity loss. The improved particle morphology of GNP-Li_xMnO_2 compensates for the slow diffusion at the end of discharge, and decreases the likelihood that over-reduction will occur, while simultaneously improving utilization at moderate to high current densities.

The abuse-tolerance, good thermal stability, remarkable cyclability, and high rate capability of GNP-Li_xMnO_2 indicate that this material would be highly suitable for use in HEV batteries, which must undergo thousands of rapid, shallow cycles at high discharge rates during normal use. Li_xMnO_2 in the as-made state is in the partially reduced state (x is estimated to be 0.3-0.44, depending upon the preparation method), and is initially charged about 15-40 mAh/g, depending upon upper voltage limit and sample and cell type, prior to the first discharge. Thus, Li_xMnO_2 made from $Na_{0.44}MnO_2$ can, in principal, be used as-is in a lithium ion battery configuration for applications not requiring high energy density such as HEVs (lithium ion batteries have been selected by the Partnership for a New Generation of Vehicles (PNGV) as candidates for this purpose).

At present, the reversible capacity of 100-120 mAh/g is somewhat low for this compound to be useful in conventional or EV batteries. The theoretical capacity is about 200 mAh/g for Li intercalation into Li_xMnO_2 with the $Na_{0.44}MnO_2$ structure[20] corresponding to a composition range of x=0-0.66. (This assumes that intercalation is site-limited, as it is in the case of Na insertion into $Na_{0.44}MnO_2$; however, there is evidence that more of the smaller Li ions can be inserted into this structure, under some conditions).[12] When used in a sodium/polymer configuration, $Na_{0.44}MnO_2$ delivers up to 150 mAh/g,[21] and, in a lithium/polymer cell, partially exchanged materials can deliver up to 180 mAh/g (140 mAh/g in the reversible region above 2.5V).[11, 12] Complete ion

exchange has the effect of steepening the discharge profile of compounds with the $Na_{0.44}MnO_2$ structure, making it difficult to extract lithium ions fully without oxidizing the electrolyte solution and compromising cycle life. Thus, the utilization during voltage-limited cycling is lower for Li_xMnO_2 than it is for $Li_xNa_yMnO_2$ or $Na_{0.44}MnO_2$. The fact that greater capacities under similar discharge conditions can be achieved for several modifications of this structure indicate that the 100-120 mAh/g obtained during discharge of Li_xMnO_2 below the oxidative stability limits of commonly used electrolyte solutions is not an inherent limitation. In fact, reversible capacities in lithium/polymer cells are increased 20% for fully exchanged active materials in which 22% of the manganese has been replaced with titanium.[22] This indicates that it is possible to modify the discharge characteristics of this structure by ad-metal doping to flatten the discharge profile, allowing more lithium to be extracted at voltages compatible with other cell components. Work in this laboratory is now directed towards understanding the effects of ad-metal doping on this material, so that increased discharge capacity can be obtained without sacrificing the excellent rate capability or cyclability seen in GNP-Li_xMnO_2.

Conclusions

Li_xMnO_2 electrodes with the $Na_{0.44}MnO_2$ structure have been discharged and cycled in lithium/liquid electrolyte cells at room temperature and in lithium/polymer cells at 85° C. Higher utilization and a dramatic improvement in rate capability is seen when a material derived from a glycine-nitrate combustion synthesis precursor is used (GNP-Li_xMnO_2) rather than one made via a conventional solid state technique (SS-Li_xMnO_2). This is attributable to the particle morphology of the former, which consists of much

shorter needles than the latter. GNP-Li_xMnO_2 has been cycled over 250 times at varying current densities, in a liquid electrolyte cell, and 140 times in a polymer cell heated to 85° C, at 1.5C rate, without any appreciable capacity fading. Furthermore, nearly full utilization is seen in Li/1M $LiPF_6$ EC-DMC/GNP-Li_xMnO_2 cells discharged up to 5C rate several times, without damage to the electrode. The outstanding cycling at both room temperature and elevated temperatures, meta-stability, and ability to withstand abuse situations and high-rate discharge make this manganese oxide a promising candidate for hybrid electric vehicle batteries, with the attendant severe performance demands.

Acknowledgments

This work was supported by the Assistant Secretary for Energy Efficiency and Renewable Energy, Office of Transportation Technologies, Office of Advanced Automotive Technologies of the U.S. Department of Energy under Contract No. DE-AC03-76SF00098. We would like to thank Dr. Xiao-Feng Zhang of the Materials Sciences Division for providing TEM images and for helpful discussion.

References

1. Chemical Marketing Reporter, 1/10/00.

2. See http://www.ta.doc.gov/pngv/goals/pp_toc.htm.

3. J. Cho and M. M. Thackeray, *J. Electrochem. Soc.*, **146**, 3577 (1999).

4. S. J. Wen, T. J. Richardson, L. Ma, K.A. Streibel, P.N. Ross, Jr., and E. J. Cairns, *J. Electrochem. Soc.*, **143**, L136 (1996).

5. A. Blyr, C. Sigala, G. Amatucci, D. Guyomard, Y. Chabre, and J. M. Tarascon, *J. Electrochem. Soc.*, **145**, 194 (1998).

6. M. M. Thackeray, S. Yang, A. J. Kahaian, K. D. Kepler, E. Skineer, J. T. Vaughey, and S. A. Hackney, *Electrochem. Solid-State Lett.*, **1**, 7 (1998).

7. A. R. Armstrong and P.G. Bruce, *Nature,* **381**, 499 (1996).

8. F. Zhang and M. S. Whittingham, *Electrochem. Solid-State Lett.*, **3**, 7 (2000).

9. S. Whittingham, personal communication.

10. J. M. Paulsen, C. L. Thomas, J. R. Dahn, *J. Electrochem. Soc.* **146**, 3560 (2000).

11. M. M. Doeff, M. Y. Peng, Y. Ma, and L. C. De Jonghe, *J. Electrochem. Soc.*,**141**, L145 (1994).

12. M. M. Doeff, T. J. Richardson, and L. Kepley, *J. Electrochem. Soc.*, **143**, 2507 (1996).

13. A. R. Armstrong, H. Huang, R. A. Jennings, and P. G. Bruce, *J. Mater. Chem.*, **8**, 255 (1998).

14. T. J. Richardson and P. N. Ross, *194th Electrochem. Society Meeting*, Boston, MA 1998, Vol. 98-2, Abstract No. 130.

15. L. A. Chick, L.R. Pederson, G.D. Maupin, J. L. Bates, L.E. Thomas, and G. J. Exarhos, *Mat. Let.* **10**, 6 (1990).

16. X.-F. Zhang, A. Anapolsky, and M. M. Doeff, unpublished results.

17. A. Anapolsky, Master's Thesis, University of California, Berkeley CA, 2000.

18. L. Edman, M. M. Doeff, A. Ferry, J. Kerr, and L. C. De Jonghe, *J. Phys. Chem. B.*,**104**, 3476 (2000).

19. M. M. Doeff, A. Ferry, Y. Ma, L. Ding and L. C. De Jonghe, *J. Electrochem. Soc.*, **144**, L20 (1997).

20. M. M. Doeff, T. J. Richardson, K. T. Hwang, and A. Anapolsky, *Proc. Electrochem. Soc.*, **99-24**, 48 (2000).

21. M. M. Doeff, L. Ding and L. C. De Jonghe, *Mat. Res. Soc. Proc.*, **393**, 107 (1995).

22. M. M. Doeff, T. J. Richardson, K.-T. Hwang and A. Anapolsky, *ITE Battery Lett.* submitted.

Figure Captions

1) Structure of Li_xMnO_2 made from $Na_{0.44}MnO_2$, looking down the c-axis.

2) Differential capacity vs. potential for a Li/1M $LiPF_6$ EC-DMC/SS-Li_xMnO_2 cell at room temperature, obtained by a stepped potential experiment. The lower trace shows data for cell discharge to 2.5V and the upper trace for cell charge to 3.8V.

3) Relative diffusion coefficients as a function of state-of-charge for the cell in Figure 2, calculated by applying the Cottrell equation to i vs t data obtained for each 10 mV step (upon discharge) from the stepped potential experiment. No numerical values for the diffusion coefficients are included because of the porous nature of the electrode.

4) A pseudo open-circuit potential profile (—) of a Li/1M $LiPF_6$ EC-DMC/SS-Li_xMnO_2 cell derived from integration of the data in Figure 2, and discharges at 0.5 mA/cm^2 of a Li/1M $LiPF_6$ EC-DMC/SS-Li_xMnO_2 cell (-----) and a Li/1M $LiPF_6$ EC-DMC/GNP-Li_xMnO_2 (·····) cell at room temperature.

5) Scanning electron micrographs of a) SS-Li_xMnO_2 and b) GNP-Li_xMnO_2.

6) Transmission electron micrograph of SS-Li_xMnO_2. Each segment of the S-shaped tunnel is 2.97 Å in length.

7) Discharges of a Li/1M $LiPF_6$ EC-DMC/GNP-Li_xMnO_2 cell at 80 $\mu A/cm^2$ (—), 0.5 mA/cm^2 (-----), and 0.8 mA/cm^2 (·····) at room temperature.

8) Discharge number 118 of a Li/1M $LiPF_6$ EC-DMC/GNP-Li_xMnO_2 cell at 25 $\mu A/cm^2$ (—), discharge number 98 at 0.14 mA/cm^2 (-----), discharge number 121 at 0.5 mA/cm^2 (·····), and discharge number 108 at 2.5 mA/cm^2 (- · - · -). Wider voltage limits were used for these discharges than those shown in Figure 7.

9) Capacity as a function of cycle number for the same Li/1M $LiPF_6$ EC-DMC/GNP-Li_xMnO_2 cell as was used for Figures 7 and 8. 9a shows cycles 28-106 where discharges were carried out at 0.14 mA/cm^2 between 4.2 and 2.5V, except where otherwise noted. 9b shows cycles 107-214. Discharges 107-117 were carried out at 2.5 mA/cm^2 between 4.2 and 1.8V (●), discharges 118 and 119 at 25 $\mu A/cm^2$ between 4.2 and 2.5V (O), discharges 120-127 at 0.5 mA/cm^2 between 4.2 and 2.25V (Δ), discharges 128-249 at 0.5 mA/cm^2 between 4.2 and 2.4V and discharges 250-259 at 0.14 mA/cm^2 between 4.2 and 2.5V(◆). (Cycles 1-27 are not shown here because of the varied cycling conditions.)

10) Capacity as a function of cycle number for a Li/1M $LiPF_6$ EC-DMC/SS-Li_xMnO_2 cell, in which the manganese oxide sample had been attritor-milled for several hours. Discharges were carried out at 0.53 mA/cm^2 between 4.0 and 2.35V, except where otherwise noted.

11) Differential capacity vs. potential for a Li/P(EO)$_8$LITFSI/GNP-Li$_x$MnO$_2$ cell at 85° C, obtained by a stepped potential experiment. The lower trace shows data for cell discharge to 2.6V and the upper trace for cell charge to 3.5V.

12) Discharges of Li/P(EO)$_8$LiTFSI/GNP-Li$_x$MnO$_2$ cells between 3.6 and 2.5V at 85° C, at current densities of 0.1 mA/cm^2 (—), 0.2 mA/cm^2 (-----), 0.5 mA/cm^2 (·····), and 1 mA/cm^2 (-·-·-·).

13) Capacity as a function of cycle number for a Li/P(EO)$_8$LiTFSI/GNP-Li$_x$MnO$_2$ cell discharged at a current density of 0.5 mA/cm^2 between 3.6 and 2.5V at 85° C..

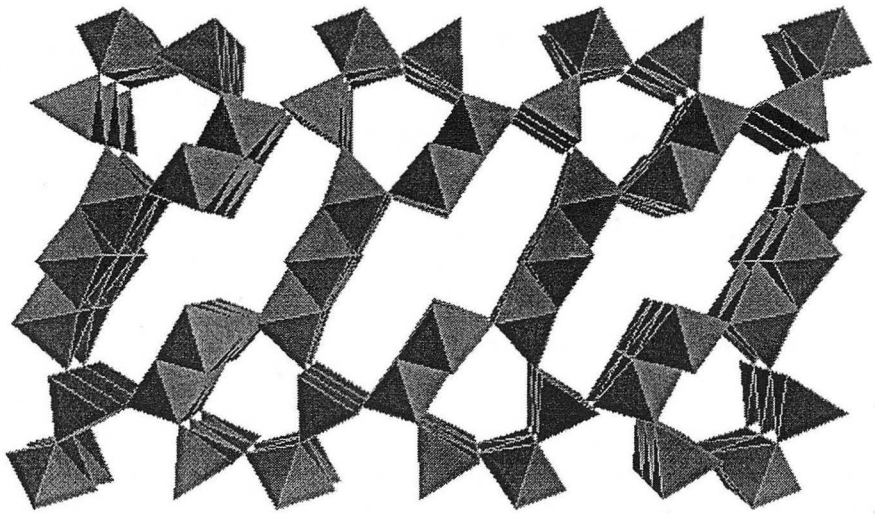

Figure 1

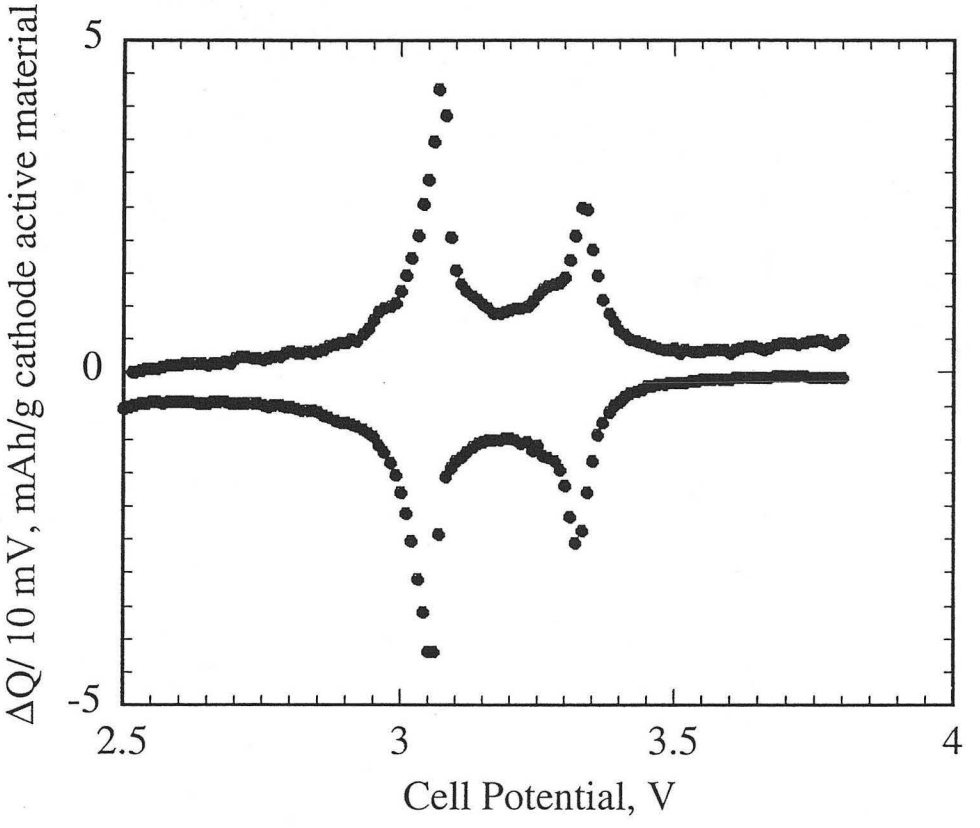
ΔQ/ 10 mV, mAh/g cathode active material
5
0
-5
2.5
3
3.5
4
Cell Potential, V

Figure 2.

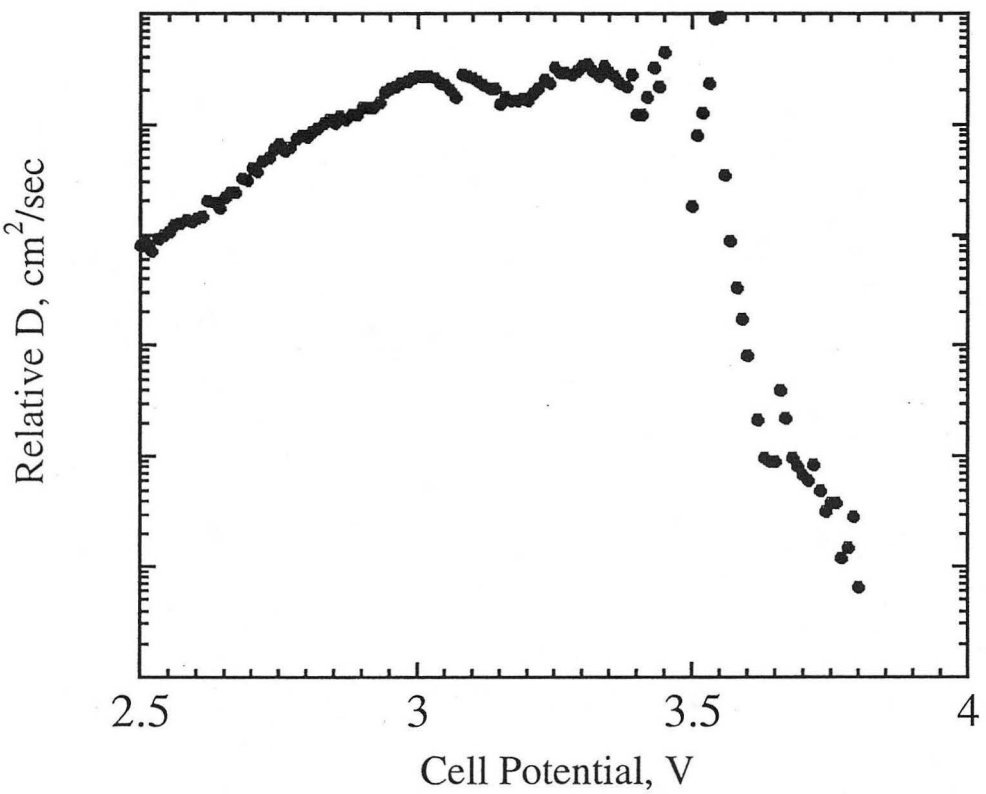

Figure 3.

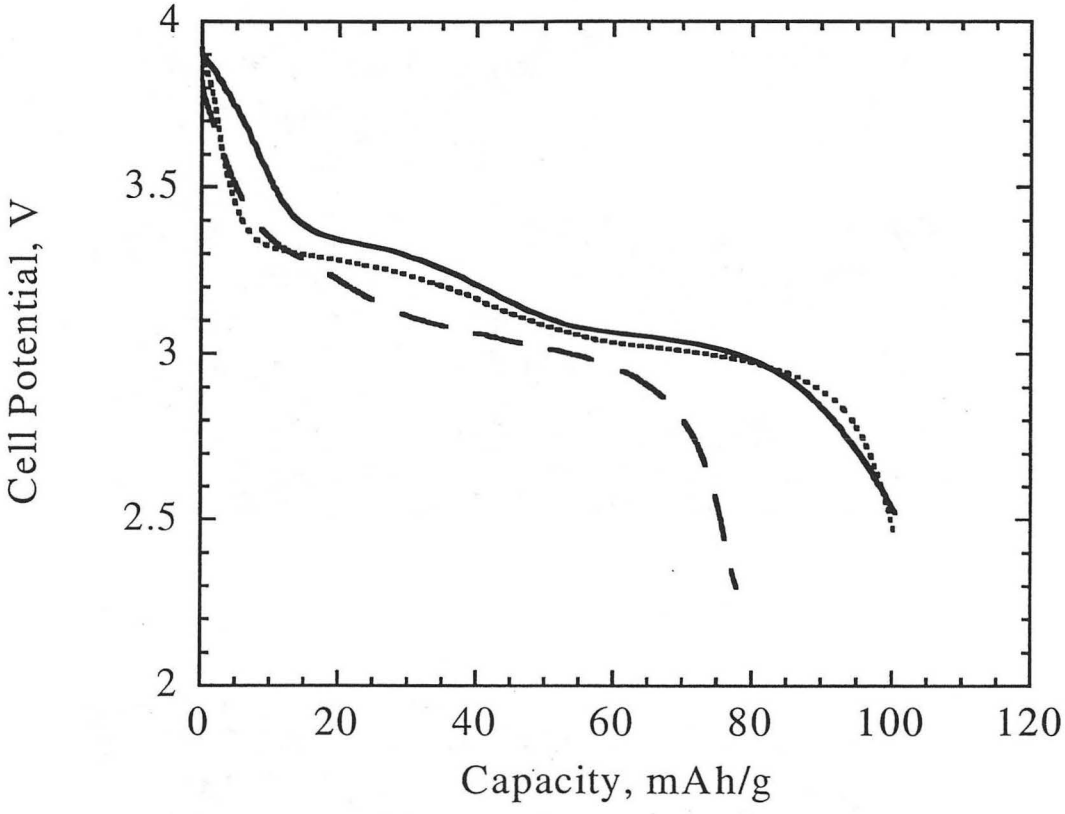

Figure 4.

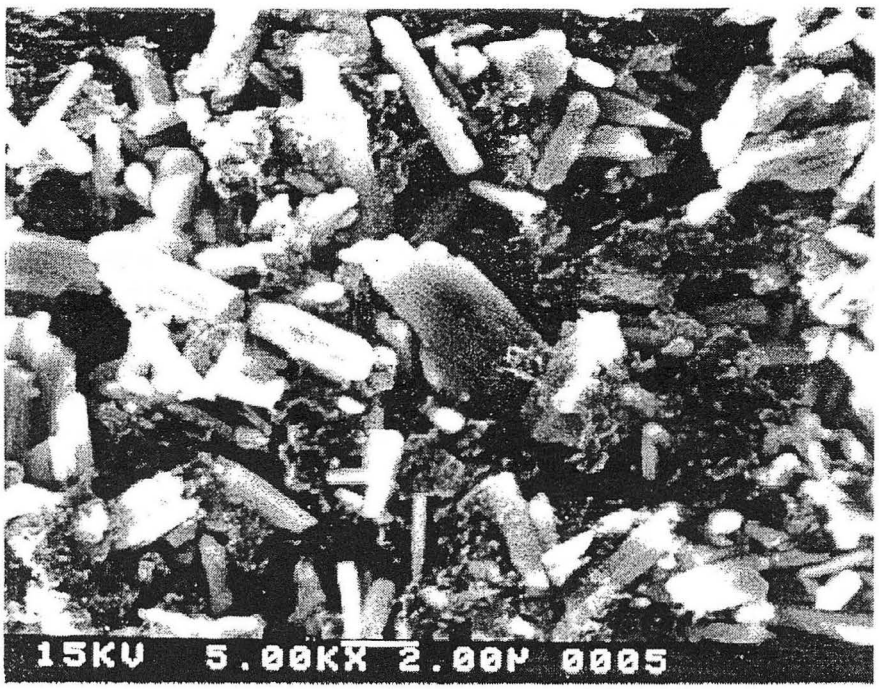

Figure 5a.

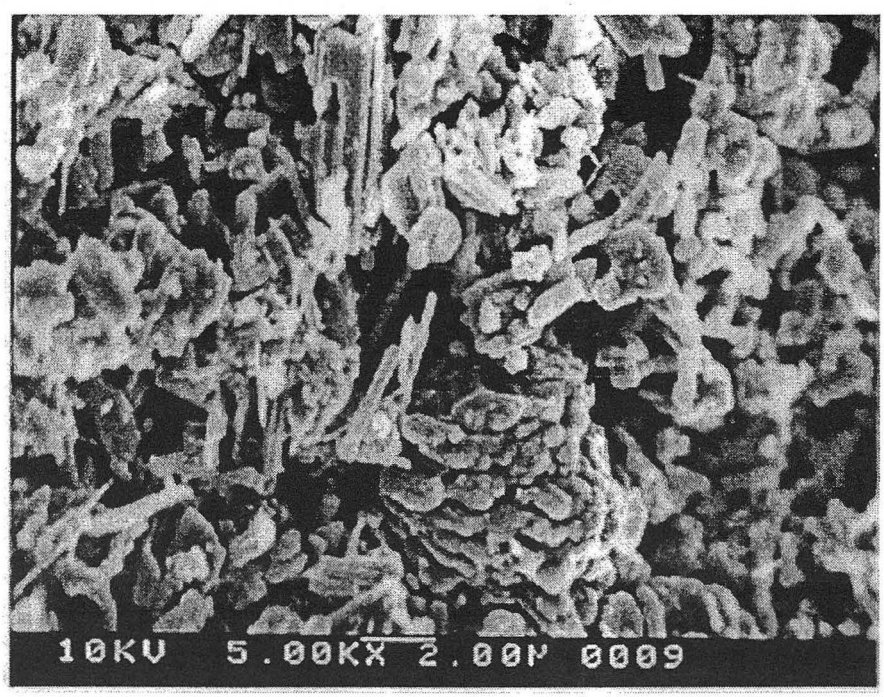

Figure 5b

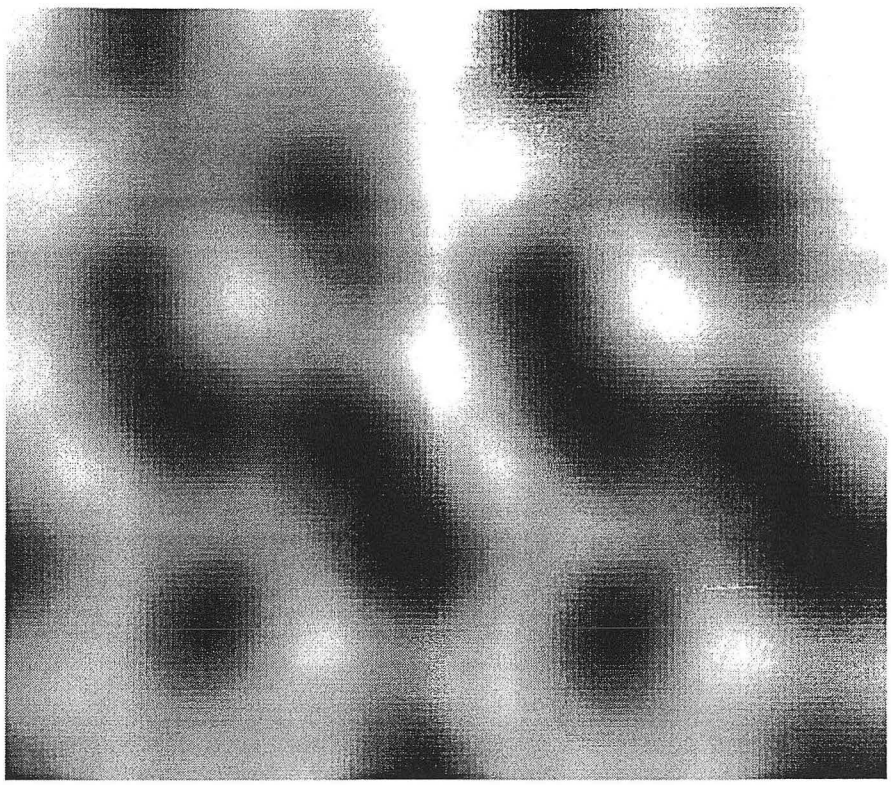

Figure 6.

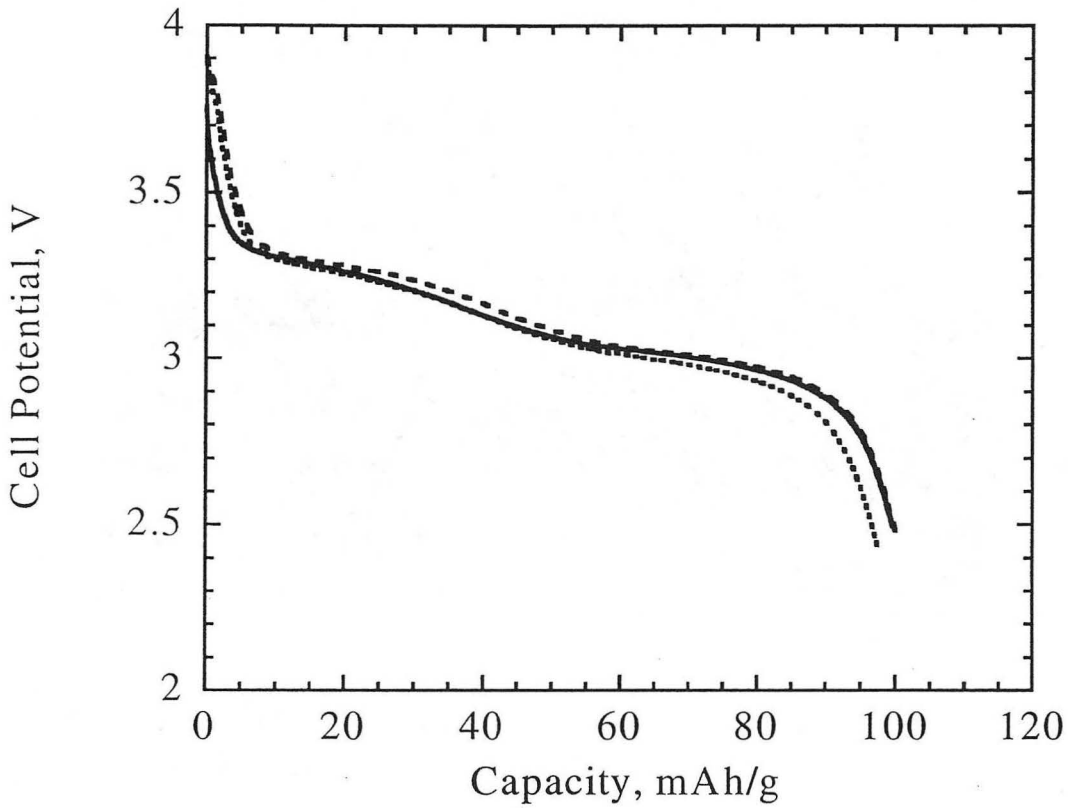

Figure 7.

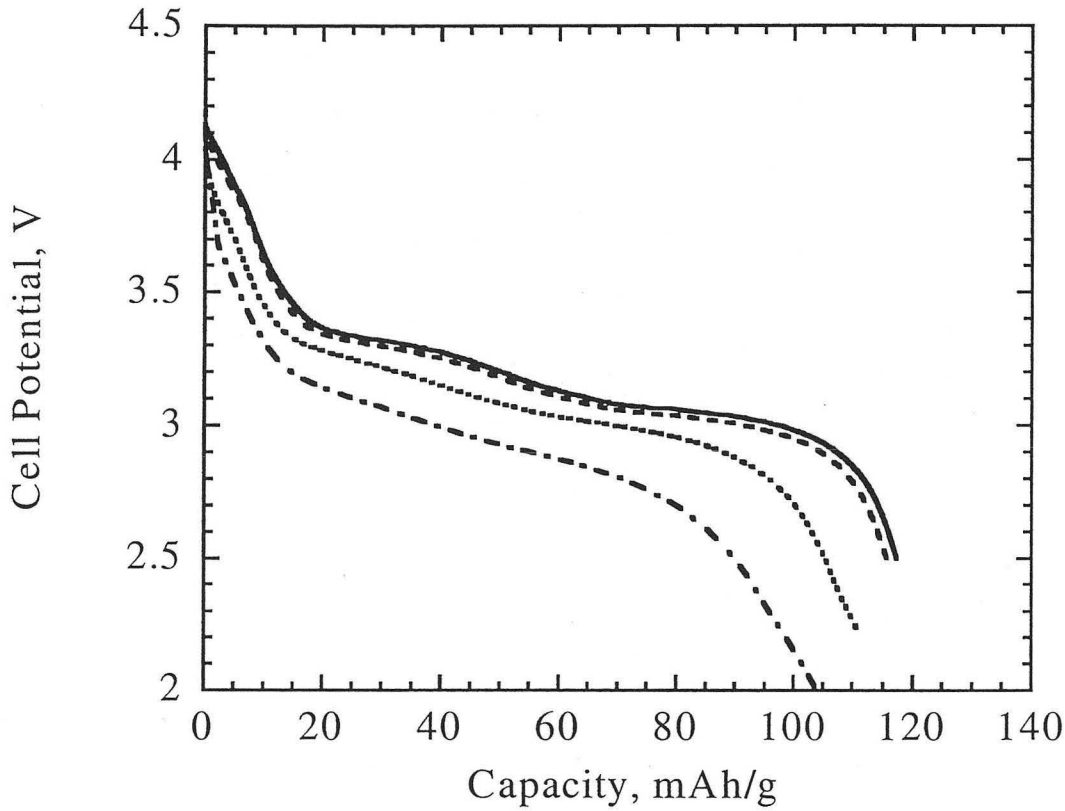
4.5
4
3.5
3
2.5
2
Cell Potential, V
0
20
40
60
80
100
120
140
Capacity, mAh/g

Figure 8.

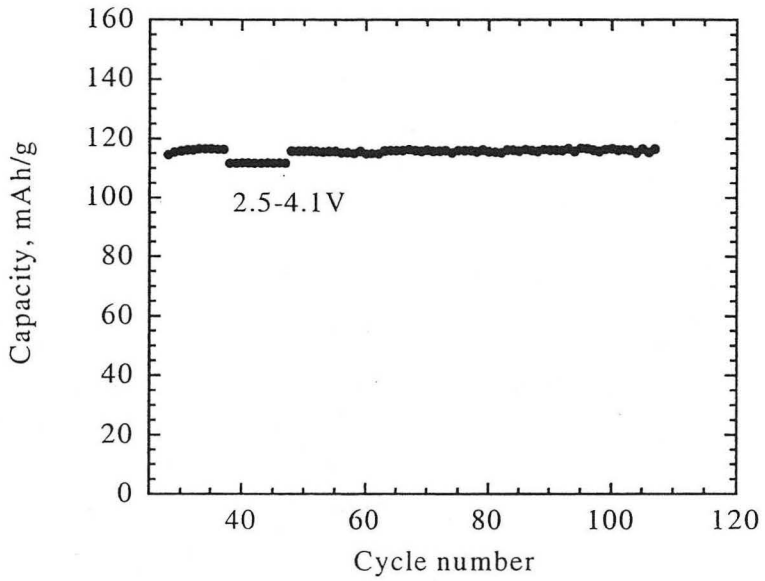

Figure 9a.

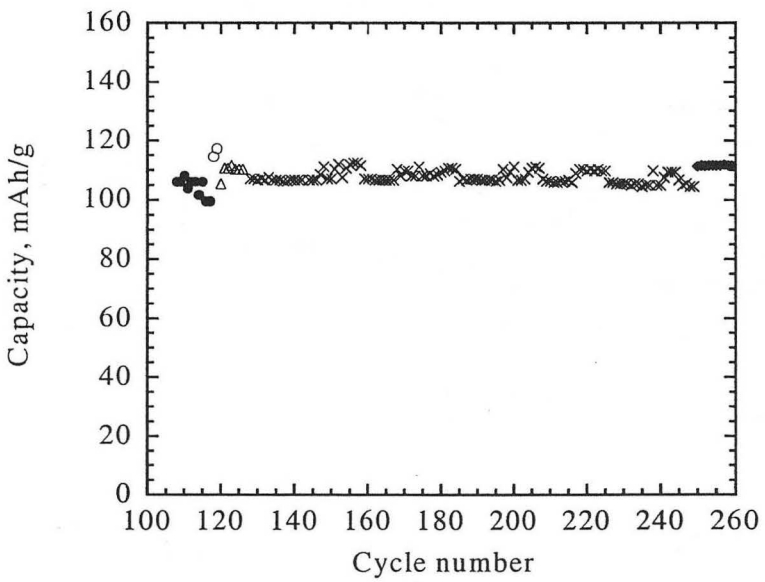

Figure 9b.

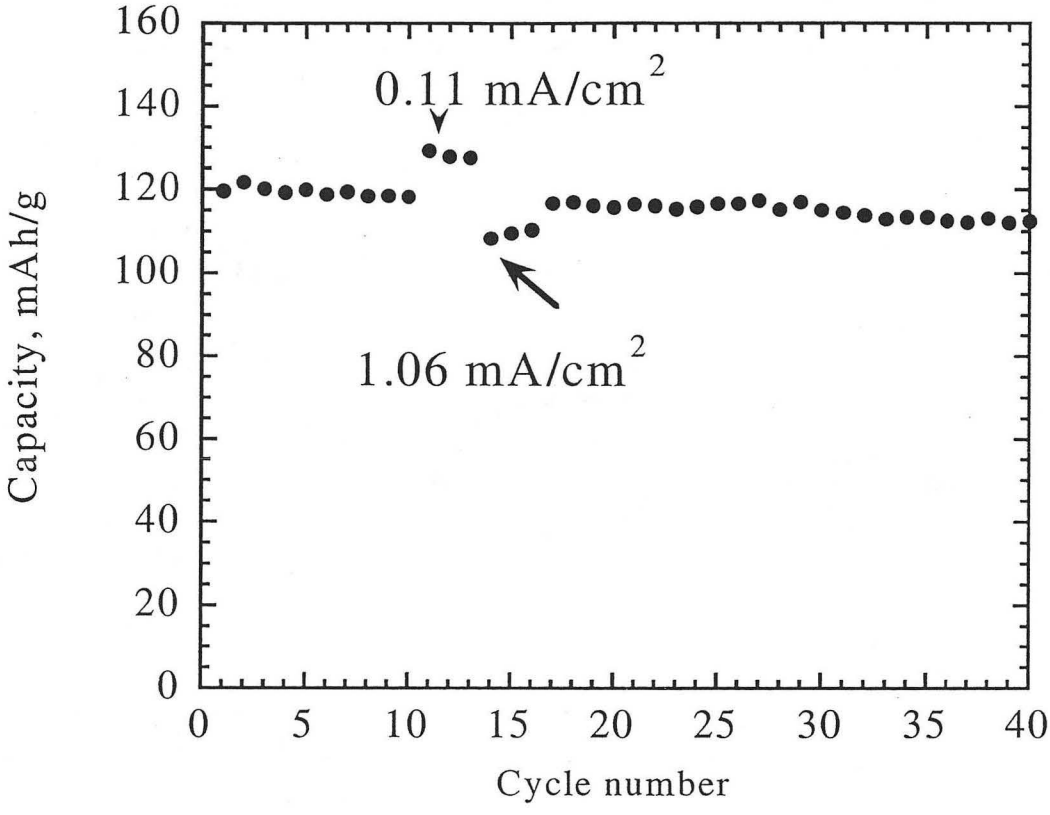
160
140
120
100
80
60
40
20
0
0.11 mA/cm2
1.06 mA/cm2
Capacity, mAh/g
0
5
10
15
20
25
30
35
40
Cycle number

Figure 10.

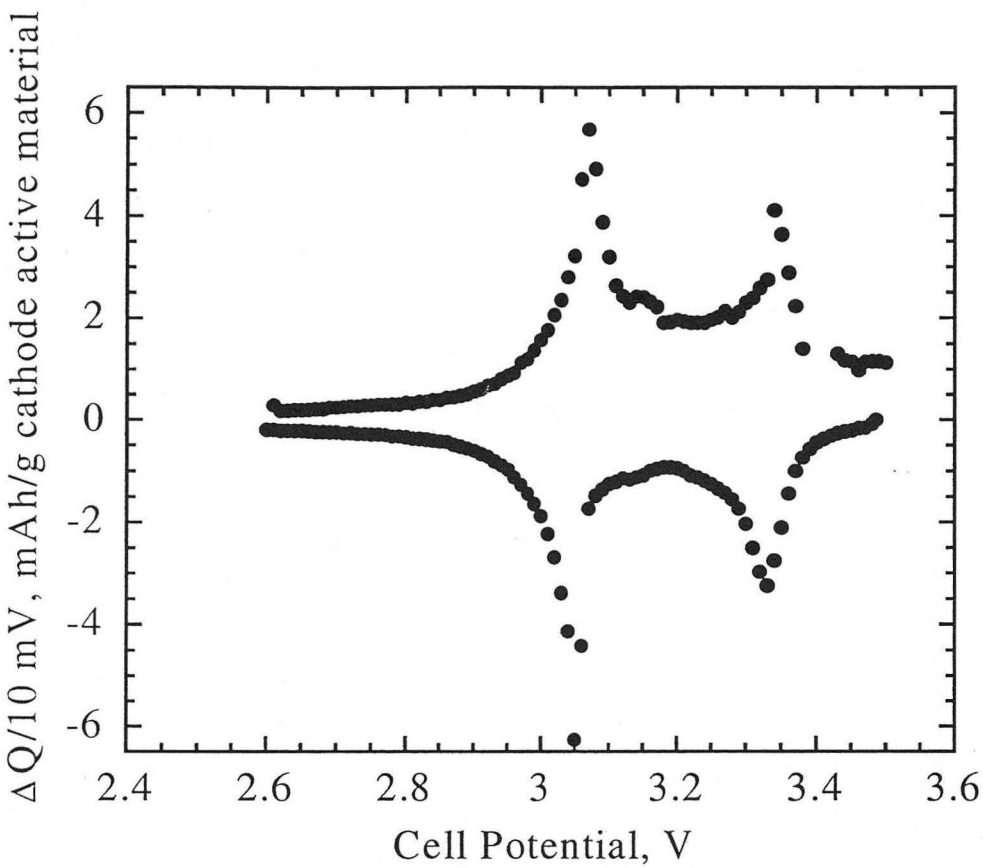
ΔQ/10 mV, mAh/g cathode active material
6
4
2
0
-2
-4
-6
2.4
2.6
2.8
3
3.2
3.4
3.6
Cell Potential, V

Figure 11.

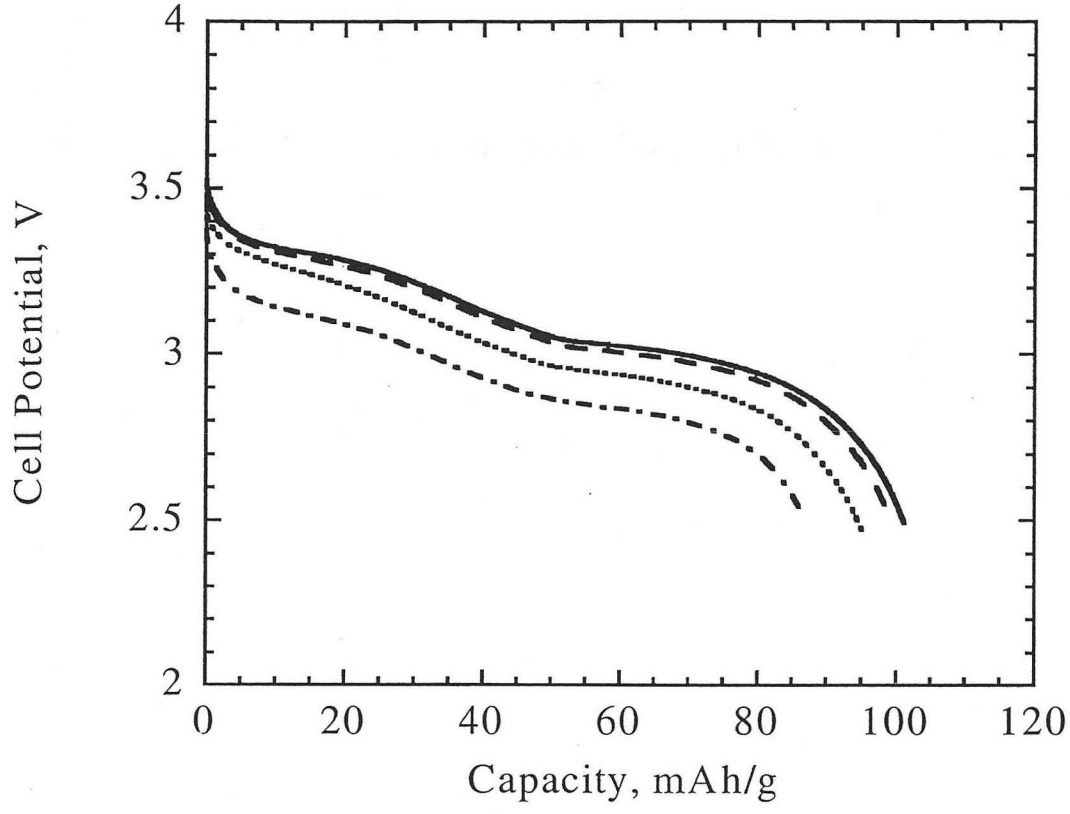

Figure 12.

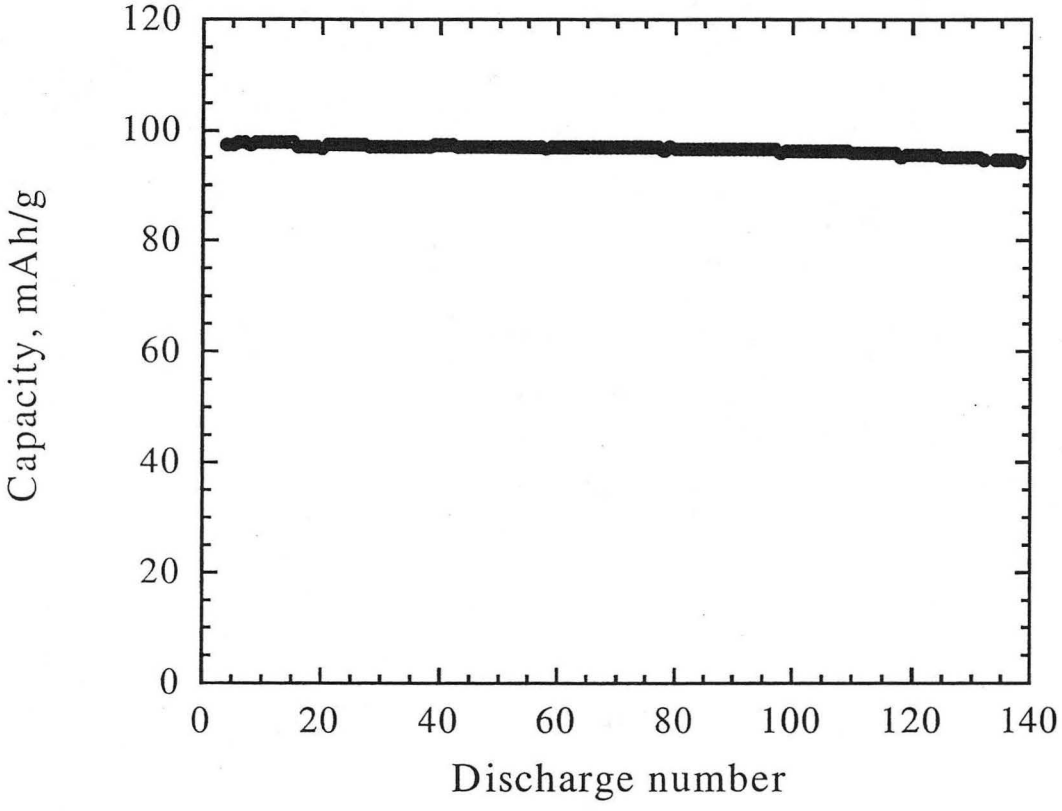
120
100
80
60
40
20
0
Capacity, mAh/g
0
20
40
60
80
100
120
140
Discharge number

Figure 13.

Ernest Orlando Lawrence Berkeley National Laboratory
One Cyclotron Road | Berkeley, California 94720

Prepared for the U.S. Department of Energy under Contract No. DE-AC03-76SF00098